ELSEVIER

www.elsevier.nl/locate/jorganchem

Journal of Organometallic Chemistry 611 (2000) 288–298

Journal of Organometallic Chemistry

Review

Bonding nature and reaction behavior of inter-element linkages with transition metal complexes. A theoretical study

Shigeyoshi Sakaki [a,*], Bishajit Biswas [a], Yasuo Musashi [b], Manabu Sugimoto [a]

[a] *Department of Applied Chemistry and Biochemistry, Faculty of Engineering, Kumamoto University, Kurokami, Kumamoto 860-8555, Japan*
[b] *Information Processing Center, Kumamoto University, Kurokami, Kumamoto 860-8555, Japan*

Received 24 March 2000; accepted 21 April 2000

Abstract

The B–C bond in $(HO)_2B–CH_3$ is stronger than the C–C bond in ethane, because a hyperconjugation interaction is formed between boryl p_π orbital and C–H bonding orbital of CH_3. The M–$B(OH)_2$ bond (M = Pd or Pt) is also stronger than the M–CH_3 bond, because of the presence of back-donating interaction between M d_π and boryl p_π orbitals and the considerably large orbital overlaps between $B(OH)_2$ sp^2 and M valence orbitals. Also, the M–XH_3 bond (X = C, Si, Ge, or Sn) becomes weaker in the order M–SiH_3 > M–GeH_3 > M–SnH_3 > M–CH_3. This result is easily interpreted in terms of the energy level and the expansion of the XH_3 sp^3 orbital. In the activation reaction of the $(HO)_2B–XH_3$ σ-bond, the empty p_π orbital of the boryl group forms the charge-transfer interaction with the M d_π orbital in the transition state (TS), to stabilize the TS and as a result to facilitate σ-bond activation. The allyl–methyl reductive elimination of $Pd(CH_3)(\eta^3\text{-}C_3H_5)(PH_3)$ requires a very large activation energy, in spite of the very large exothermicity. On the other hand, allyl–silyl, allyl–germyl, and allyl–stannyl reductive eliminations occur with a moderate activation barrier, while they are moderately exothermic (X = Si or Ge) or moderately endothermic (X = Sn). This difference between methyl and the others is clearly interpreted in terms of the presence of hypervalency of silyl, germyl, and stannyl elements.

Keywords: Ab initio calculation; B–C bond; B–Si bond; B–Ge bond; B–Sn bond; Transition metal–boryl bond; Transition metal–silyl bond; Transition metal–germyl bond; Transition metal–stannyl bond; Hypervalency; Hyperconjugation; σ-Bond activation; η^3-Allyl reductive elimination

1. Introduction

The introduction of boryl, silyl, germyl, and stannyl groups into organic substrates is an interesting and important reaction, since the products of such introduction reactions are key intermediates in various organic syntheses. In the introduction reactions, inter-element linkages which consist of boryl, silyl, germyl, and stannyl groups undergo σ-bond activation by transition metal complexes in general. Typical examples are transition metal-catalyzed hydrosilylation [1] and hydroboration [2] which take place through Si–H and B–H σ-bond activation reactions by transition metal complexes, respectively. Also, σ-bond activation reactions of Si–Si [3], B–B, and similar bonds [4] have received considerable interest because these reactions are useful to introduce two functional groups such as silyl [5–8], boryl [4], and similar groups [9,10] into organic compounds. To perform efficiently this type of σ-bond activation reaction, detailed knowledge of the bonding nature and reaction behavior of inter-element linkages is necessary. However, little is known about the bonding nature, bond strength, and reaction behavior of the inter-element linkages with transition metal complexes.

Theoretical methods such as ab initio MP2-MP4, CCSD(T), and DFT methods are useful and helpful for investigating the bonding nature, the bond strength, and the reaction behavior of inter-element linkages. In

* Corresponding author. Tel.: +81-96-342-3651; fax: +81-96-342-3679.
E-mail address: sakaki@gpo.kumamoto-u.ac.jp (S. Sakaki).

0022-328X/00/$ - see front matter
PII: S0022-328X(00)00456-3

particular, theoretical methods can provide valuable and important information about transition states of organometallic reactions and catalytic reactions by transition metal complexes, while it is difficult to present such information experimentally. We believe that theoretical knowledge of transition state and electronic processes of the reaction is indispensable to understand well the characteristic features of inter-element linkages. In fact, many theoretical works provided detailed knowledge of the C–H and C–C σ-bond activation reactions [11–14].

Recently, we have carried out several theoretical studies of σ-bond activation reactions of C–H, Si–C, and B–X (X = C, Si, Ge, or Sn) bonds by Pt(0) and Pd(0) complexes [15–17], in which we estimated the bond energy of transition metal–alkyl, silyl, germyl, stannyl, and boryl bonds, optimized transition state structures, and evaluated the activation energy and reaction energy of those reactions. Through these theoretical works, we elucidated the characteristic features of the σ-bond activation reactions of inter-element linkages by transition metal complexes, and clarified what factors are important for the reaction. In this account, we wish to summarize these results, in an attempt to present theoretical details concerning the bond strength, the bonding nature, and the reaction behavior of inter-element linkages. First, we discuss characteristic features of boryl–methyl, boryl–silyl, boryl–germyl, and boryl–stannyl bonds, and then present comparisons among the M–alkyl, silyl, germy, and stannyl bonds (M = Pd or Pt). Finally, we show clearly the reaction behavior of inter-element linkages and discuss this from the point of view of contributions of hypervalency of Si, Ge, and Sn elements and the vacant p_π orbital of the boryl group. Also, we theoretically investigated the reaction mechanism of Pt-catalyzed hydrosilylation of ethylene [18] and the insertion reactions of ethylene and acetylene into the Pt–silyl and Pt–H bonds [19]. However, we omit these results here, since our review article published recently covers most of those results [18c].

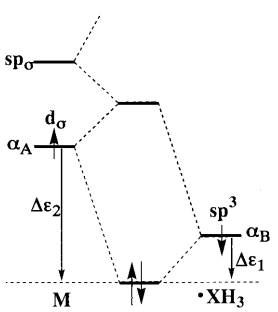

Scheme 1.

2. General consideration of bond strength

Let us consider first the interaction between two orbitals. When the M d_σ orbital is at a much higher energy than the XH_3 sp^3 orbital, as shown in Scheme 1, orbital stabilization energies ($\Delta\varepsilon_1$ and $\Delta\varepsilon_2$) are represented by Eqs. (1) and (2), according to a simple molecular orbital theory, where ε_A and ε_B represent orbital energies of M d_σ and XH_3 sp^3 orbitals, respectively, and β is the usual resonance integral. Thus, a total bond stabilization energy $\Delta\varepsilon_{cov}$ by covalent bond formation is given by Eq. (3) [15b].

$$\Delta\varepsilon_1 = \beta^2/(\varepsilon_A - \varepsilon_B) \quad (1)$$

$$\Delta\varepsilon_2 = (\varepsilon_A - \varepsilon_B) + \beta^2/(\varepsilon_A - \varepsilon_B) \quad (2)$$

$$\Delta\varepsilon_{cov} = \Delta\varepsilon_1 + \Delta\varepsilon_2 = (\varepsilon_A - \varepsilon_B) + 2\beta^2/(\varepsilon_A - \varepsilon_B) \quad (3)$$

If the $|\beta|$ value is smaller than $2(\varepsilon_A - \varepsilon_B)$, the $\Delta\varepsilon_{cov}$ value becomes larger as the $(\varepsilon_A - \varepsilon_B)$ value increases; in other words, the bond energy increases as M d_σ and XH_3 sp^3 orbitals become more separate in energy. The meaning of Eq. (3) is essentially the same as the proposal by Pauling that the covalent bond becomes stronger as the ionic character increases. The other factor is the resonance integral β; when the $|\beta|$ value is small, the bond stabilization energy is small. Based on these two factors, we will discuss the bond strength hereafter.

Eq. (3) was successfully applied to explain why an electron-withdrawing substituent strengthens the Pd–alkyl bond. It is believed in general that introduction of an electron-withdrawing substituent on an sp^3 carbon atom strengthens the metal–alkyl bond. However, this tendency has not been clearly explained yet, to our knowledge.

Here, we theoretically evaluated the Pd–alkyl bond energy with the MP4(SDQ) method, by considering the following equation:

$$cis\text{-PdH(alkyl)}(PH_3)_2 \rightarrow Pd(PH_3)_2 + \text{H-alkyl} \quad (4)$$

An energy difference $\Delta E_{r\text{-}l}$ between the left-hand and the right-hand sides of Eq. (4) is represented with bond energies as follows:

$$\Delta E_{r\text{-}l}(\text{Eq. (4)}) = E_t(\text{right-hand side}) - E_t(\text{left-hand side}) = E(\text{Pd–H}) + E(\text{Pd–alkyl}) - E(\text{H–alkyl}) \quad (5)$$

where E(Pd–H), E(Pd–alkyl), and E(alkyl–H) represent the Pd–H, Pd–alkyl, and H–alkyl bond energies, respectively. E(Pd–H) is evaluated with the assumed Eq. (6);

$$cis\text{-PdH}_2(PH_3)_2 \rightarrow Pd(PH_3)_2 + 2H \quad (6)$$

$$\Delta E_{r\text{-}l}(\text{Eq. (6)}) = 2E(\text{Pd–H}) - E(\text{H–H}) \quad (7)$$

Table 1
C–H and Pd(II)–alkyl bond energies [a]

System	Bond	Energy
CH_4	E(C–H)	108.6
CH_3CN	E(C–H)	106.4
$CH_2(CN)$	E(C–H)	104.4
cis-$PdH(CH_3)(PH_3)$	E(Pd–CH_3)	21.2
cis-$PdH(CH_2(CN))(PH_3)$	E(Pd–CH_2(CN))	30.9
cis-$PdH(CH(CN)_2)(PH_3)$	E(Pd–$CH(CN)_2$)	40.1

[a] MP4(SDQ) in kcal mol^{-1}.

Table 2
The B–X bond energy in $(HO)_2B–XH_3$ (X = C, Si, Ge, or Sn) [a]

B–B [b]	103.6		
B–C	109.7	C–C	91.6
B–Si	86.8	C–Si	86.0
B–Ge	83.5	C–Ge	79.3
B–Sn	72.8	C–Sn	73.6

[a] MP4(SDQ) in kcal mol^{-1}.
[b] In $(HO)_2B–B(OH)_2$ [24].

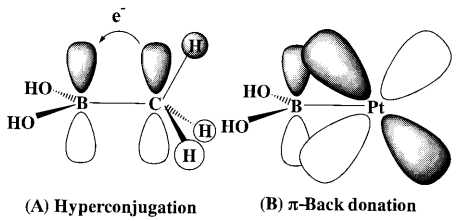

Scheme 2.

We call the above-estimated E(Pd–alkyl) value an averaged bond energy, and represent it as E_{av}. As shown in Table 1, the Pd–alkyl bond energy increases in the order $Pd–CH_3 < Pd–CH_2CN < Pd–CH(CN)_2$ [15b]. This increasing order is consistent with the understanding that an electron withdrawing substituent on the sp^3 carbon atom strengthens the metal–alkyl bond. The d orbital energy of $^{\bullet}PdH(PH_3)_2$ was calculated to be -6.6 eV, and the alkyl sp^3 orbital energy was -11.5 eV for $^{\bullet}CH_3$, -12.5 eV for $^{\bullet}CH_2(CN)$, and -13.3 eV for $^{\bullet}CH(CN)_2$. According to Eq. (3), the bond stabilization energy increases in the order $Pd–CH_3 < Pd–CH_2CN < Pd–CH(CN)_2$, since the $(\varepsilon_A - \varepsilon_B)$ value increases in the order $^{\bullet}CH_3 < ^{\bullet}CH_2CN < ^{\bullet}CH(CN)_2$. These results clearly show that Eq. (3) is useful to discuss bond strengths of transition metal–alkyl and similar bonds.

3. Bond strengths and characteristic features of boryl–methyl, boryl–silyl, boryl–germyl and boryl–stannyl bonds

Reductive elimination of the boryl–alkyl bond is involved in transiton metal-catalyzed hydroboration of alkene [2]. Also, σ-bond activation reactions of boryl–silyl and boryl–stannyl bonds are believed to be involved in silylboration and stannylboration of alkene and alkyne [9,10]. In this regard, bond strength information of boryl–methyl, boryl–silyl, and similar bonds is fundamental to a good understanding of the above-mentioned reactions. Theoretically estimated bond energies are listed in Table 2. Interestingly, the boryl–methyl and boryl–boryl bonds are much stronger than the methyl–methyl bond by about 20 kcal mol^{-1}. This is surprising because it was experimentally [4] and theoretically [20] reported that the platinum(0) complex could activate the B–B σ-bond rather easily whereas C–C σ-bond activation by platinum(0) complexes is much more difficult [12,15a].

One of the characteristic features of the boryl group is the presence of an empty p_π orbital, while the methyl group does not have such an empty p_π orbital. This empty p_π orbital can form a hyperconjugation interaction with an occupied C–H bonding orbital of the methyl group, as schematically shown in Scheme 2A. Actually, the HOMO of methylborane involves a bonding interaction between boryl p_π and C–H bonding orbitals, as shown in Fig. 1B [17]. Consistent with this bonding interaction, the electron population of the boryl p_π orbital is larger in methylborane than in the free boryl radical, as shown in Table 3, where the natural bond orbital population analysis [21] is adopted. This hyperconjugation is responsible for the fact that the B–C bond of $(HO)_2B–CH_3$ is stronger than the C–C bond of ethane. The energy difference between CH_3 sp^3 and $B(OH)_2$ sp^2 orbitals should be taken into consideration also. The C–C bond is a non-polar covalent bond. In methylborane, on the other hand, the B–C bond is a polar bond that consists of the overlap between boryl sp^2 and CH_3 sp^3 orbitals, where the former is at a lower energy than the latter. In a comparison between the C–C and B–C bonds, Eq. (3) is not useful, since the $\varepsilon_A - \varepsilon_B$ value is small in the B–C bond and equal to zero in the C–C bond. However, a slightly more complicated equation is obtained when the $\varepsilon_A - \varepsilon_B$ value is small, which also indicates that the bond stabilization energy increases with an increase of the $\varepsilon_A - \varepsilon_B$ value [22]. This means that the energy difference between boryl sp^2 and CH_3 sp^3 orbitals is the other reason that the B–C bond in methylborane is stronger than the C–C bond in ethane. Detailed discussion is omitted here.

On the other hand, this hyperconjugation interaction is not observed in silylborane, germylborane, and stannylborane, as shown in Fig. 1C–E. However, the boryl p_π orbital is observed in the occupied space of these molecules, too. Consistent with this, the electron population of the boryl p_π orbital is larger in these molecules than in the free boryl group (see Table 3), and the electron populations of silyl, germyl, and stannyl

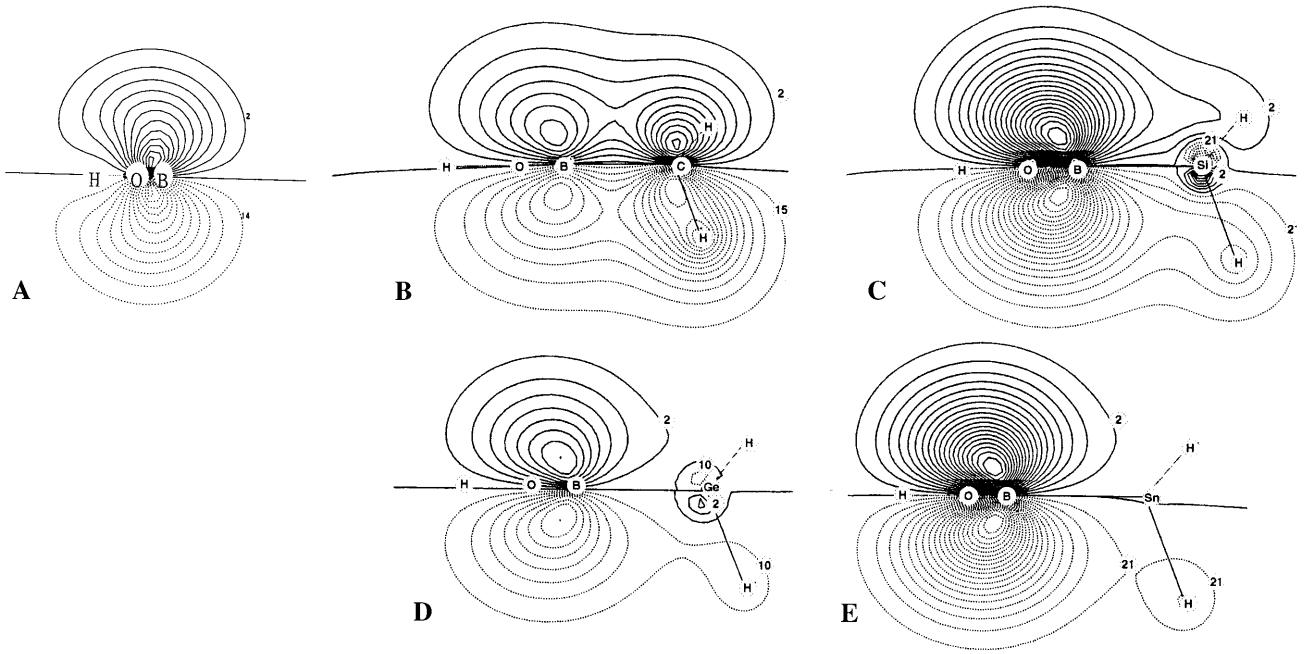

Fig. 1. Contour maps of π-type HOMO of $^{\bullet}B(OH)_2$ and $(HO)_2B–XH_3$ (X = C, Si, Ge, or Sn). Contour values increase from −0.125 by 0.0125 and decrease from 0.125 by 0.0125 in $^{\bullet}B(OH)_2$, $(HO)_2B–CH_3$, $(HO)_2B–SiH_3$, and $(HO)_2B–GeH_3$. Contour values increase from −0.05 by 0.005 and decrease from −0.05 by 0.005 in $(HO)_2B–SnH_3$.

groups are smaller than those in disilane, digermane, and distannane. These features suggest that intra-molecular charge-transfer (CT) occurs from silyl, germyl, and stannyl groups to the boryl p_π orbital. In spite of this intra-molecular CT interaction, the B–Si, B–Ge, and B–Sn bonds are as strong as the C–Si, C–Ge, and C–Sn bonds (Table 2), respectively, probably because of the absence of hyperconjugation. It is not surprising that the hyperconjugation becomes weaker in the heavy element, since the π-type overlap becomes unfavorable upon going down in the periodic table.

The considerable strength of the B–B bond of $(HO)_2B–B(OH)_2$ is also interpreted in terms of a partial π bonding nature. As previously proposed [23], diborane corresponds to the dication of ethylene, since the π orbital of diborane is empty unlike ethylene. However, the OH group has a doubly occupied p_π orbital which participates in an intra-molecular CT interaction from the OH p_π orbital to B p_π orbital [24]. As a result, the B–B bond is not a single bond but partially possesses π-bonding nature. Thus, the B–B bond of $(HO)_2B–B(OH)_2$ is stronger than the C–C bond in ethane.

The other interesting result to be noted is that the B–X bond energy of $(HO)_2B–XH_3$ decreases in the order B–C > B–Si > B–Ge > B–Sn. This decreasing order is consistent with the general tendency that the covalent bond of non-transition metal elements becomes weaker upon going down in the periodic table; actually, the C–X bond energy also decreases in the order C–C > C–Si > C–Ge > C–Sn (Table 2). This tendency is not interpreted in terms of orbital energy difference, as follows: the $^{\bullet}B(OH)_2$ radical has its sp^2 orbital at −9.6 eV, while the $^{\bullet}CH_3$ radical has its sp^3 orbital at −10.4 eV, as shown in Table 4. $^{\bullet}SiH_3$, $^{\bullet}GeH_3$, and $^{\bullet}SnH_3$ radicals have their sp^3 orbitals at −9.0, −8.9 and −8.6 eV, respectively. The energy difference is the greatest in stannylborane, while the

Table 3
Natural bond orbital population [a] of the boryl p_π orbital

$^{\bullet}B(OH)_2$	0.287		
$(HO)_2B–CH_3$	0.316	$(HO)_2B–GeH_3$	0.332
$(HO)_2B–SiH_3$	0.330	$(HO)_2B–SnH_3$	0.333

[a] Ref. [21].

Table 4
The sp^3 orbital energies (ε_{sp3}), ionization potential (I_p), and electron affinity (EA) of $^{\bullet}XH_3$ and $^{\bullet}B(OH)_2$

	ε_{sp3} [a]	I_p [a]	EA [b]
$^{\bullet}B(OH)_2$	−9.59	6.36	0.34
$^{\bullet}CH_3$	−10.5	9.52	−1.05 (−0.48) [c] [0.08] [d]
$^{\bullet}SiH_3$	−9.01	7.78	0.67 (0.78) [c] [1.41] [d]
$^{\bullet}GeH_3$	−8.97	7.71	1.06 (1.21) [c]
$^{\bullet}SnH_3$	−8.57	7.37	1.15
cis-$PdH(PH_3)$	−7.0		
cis-$PtH(PH_3)_2$	−6.8		

[a] MP4(SDQ)/6-311G**/MP2/6-31G*.
[b] MP4(SDQ)/6-311G++**/MP2/6-31++G**.
[c] Calculated with the more accurate G2 method [27].
[d] Experimental values (cited in ref. [28]).

Table 5
The first bond dissociation energy (E_{first}) and the averaged bond energy (E_{av}) of M–$B(OH)_2$ and M–XH_3 bonds in *cis*-$M(XH_3)[B(OH)_2](PH_3)_2$ (M = Pd or Pt; X = C, Si, Ge, or Sn) [a]

	E_{first}	E_{av}		E_{first}	E_{av}
Pt–$B(OH)_2$	89.1	64.4	Pd–$B(OH)_2$	77.0	52.8
Pt–CH_3	65.5	42.4	Pd–CH_3	54.3	29.4
Pt–SiH_3	78.6	54.2	Pd–SiH_3	74.6	44.1
Pt–GeH_3	75.0	50.7	Pd–GeH_3	69.8	42.3
Pt–SnH_3	71.2	46.3	Pd–SnH_3	69.7	40.3

[a] MP4(SDQ) in kcal mol^{-1}.

B–Sn bond is the weakest. Thus, it is not the orbital energy difference but another factor which is responsible for this tendency. At this moment, we cannot present a clear reason for this tendency and need to carry out more detailed examination.

4. Platinum– and palladium–boryl, methyl, silyl, germyl, and stannyl bonds

In addition to the averaged bond dissociation energy, we define here the first bond dissociation energy E_{first} by the following Eq. (8);

$$M(XH_3)L_n \rightarrow {}^{\bullet}ML_n + {}^{\bullet}XH_3 \quad (8)$$

This assumed equation corresponds to the homolytic bond fission of an M–XH_3 bond.

Both first bond dissociation and averaged bond dissociation energies are listed in Table 5. Apparently, the Pt–CH_3 bond is the weakest, and the bond energy increases in the order Pt–CH_3 < Pt–SnH_3 < Pt–GeH_3 < Pt–SiH_3 in both first bond dissociation and averaged bond dissociation energies.

The sp^3 orbital of ${}^{\bullet}XH_3$ is at a lower energy than the M d orbital in *cis*-$MH(PH_3)_2$, as shown in Table 4. This means that the Pt–XH_3 bond energy becomes larger as the sp^3 orbital of ${}^{\bullet}XH_3$ descends in energy. Thus, the sp^3 orbital energy of ${}^{\bullet}XH_3$ should be examined here as a determining factor of the bond energy. The sp^3 orbital of ${}^{\bullet}XH_3$ descends in energy in the order ${}^{\bullet}SnH_3$ > ${}^{\bullet}GeH_3$ > ${}^{\bullet}SiH_3$ > ${}^{\bullet}CH_3$ (Table 4). The low energy level of the ${}^{\bullet}CH_3$ sp^3 orbital should lead to a large M–CH_3 bond energy, according to Eq. (3). However, the M–CH_3 bond is the weakest. Here, we should consider the reason why the orbital energy is not responsible for the weak M–CH_3 bond. We must remember that the CH_3 group is much more negatively charged in the M–CH_3 bond. Moreover, though the ${}^{\bullet}XH_3$ sp^3 orbital becomes higher in energy as the ionization potential decreases, the electron affinity (EA) of ${}^{\bullet}CH_3$ is the smallest in spite of the lowest energy level of the ${}^{\bullet}CH_3$ sp^3 orbital. This means that orbital relaxation occurs considerably upon electron attachment and the orbital energy is not a good measure of energy level of the CH_3 sp^3 electron when the CH_3 group is much more negatively charged as it is in Pt(II) and Pd(II)–methyl complexes. If we adopt the EA value as a measure of the energy level of the electron, the CH_3 sp^3 electron exists at the highest energy, which leads to the smallest M–CH_3 bond energy.

Besides the orbital energy, the β value would be responsible for the bond energy difference. The β value is related to an overlap integral between XH_3 sp^3 and M valence orbitals. Comparisons of the overlap integrals among CH_3, SiH_3, GeH_3, and SnH_3 are made, as shown in Table 6. The overlap integrals of CH_3 sp^3 orbital with M nd_{z^2}, $(n+1)s$, and $(n+1)p_z$ orbitals are much smaller than those of the others, where n is 4 for Pd and 5 for Pt. These smaller overlap integrals between CH_3 sp^3 and M valence orbitals are also responsible for the smaller M–CH_3 bond energy.

The overlap integrals decrease slightly in the order $SiH_3 > GeH_3 > SnH_3$, and at the same time, the sp^3 orbital energy lowers slightly in energy in the order $SnH_3 > GeH_3 > SiH_3$. Thus, the decreasing order of the bond energy M–SiH_3 > M–GeH_3 > M–SnH_3 arises from both the orbital energy and the β value. In these bonds, SiH_3, GeH_3, and SnH_3 groups are not very negatively charged (remember that Si, Ge, and Sn atoms are much less electronegative than the C atom). Thus, the XH_3 sp^3 orbital energy is considered a reasonable measure of the energy level of the sp^3 valence electron.

The other result to be noted is that the Pd–XH_3 bond is weaker than the Pt–XH_3 bond. Though this is

Table 6
Overlap integrals between M and XH_3 and between M and $B(OH)_2$

	M = Pd			M = Pt		
	$<sp^3\|5s>$	$<sp^3\|5p_z>$	$<sp^3\|4d_{z^2}>$	$<sp^3\|6s>$	$<sp^3\|6p_z>$	$<sp^3\|5d_{z^2}>$
$B(OH)_2$	0.53	0.54	0.42	0.54	0.54	0.49
CH_3	0.34	0.33	0.32	0.36	0.34	0.36
SiH_3	0.50	0.52	0.35	0.53	0.53	0.41
GeH_3	0.51	0.53	0.34	0.47	0.48	0.34
SnH_3	0.48	0.48	0.30	0.47	0.48	0.34

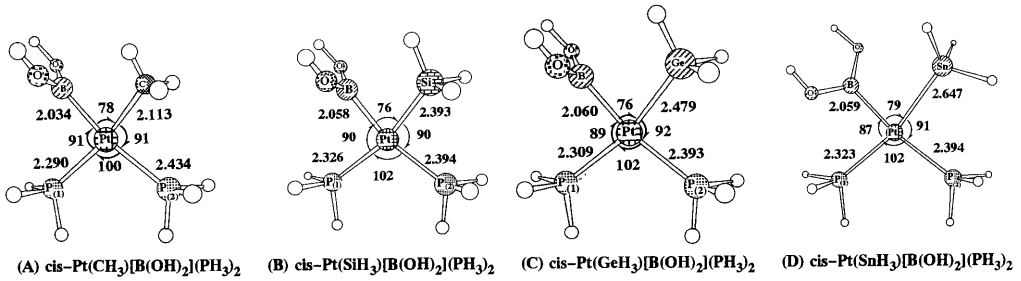

(A) cis-Pt(CH$_3$)[B(OH)$_2$](PH$_3$)$_2$ (B) cis-Pt(SiH$_3$)[B(OH)$_2$](PH$_3$)$_2$ (C) cis-Pt(GeH$_3$)[B(OH)$_2$](PH$_3$)$_2$ (D) cis-Pt(SnH$_3$)[B(OH)$_2$](PH$_3$)$_2$

Fig. 2. Optimized geometries of *cis*-Pt(XH$_3$)[B(OH)$_2$](PH$_3$)$_2$ (X = C, Si, Ge, or Sn); bond lengths in Å and bond angle in degrees.

well known, a clear explanation has not been presented yet. However, Eq. (3) provides us a clear explanation of this result, as follows: *cis*-PdH(PH$_3$)$_2$ has its d orbital at a somewhat lower energy than *cis*-PtH(PH$_3$)$_2$ (vide supra). This means that the $\varepsilon_A - \varepsilon_B$ value is smaller in *cis*-PdH(XH$_3$)(PH$_3$)$_2$ than in the Pt analog. Thus, the Pd–XH$_3$ bond is weaker than the Pt–XH$_3$ bond.

The M–B(OH)$_2$ bond is much stronger than the M–CH$_3$ bond in both M = Pd and Pt (see Table 5). It was also experimentally reported that the Ir–Bcat bond in *trans*,*cis*-IrCl(H)(Bcat)(PPh$_3$)$_2$ is as strong as the Ir–H bond in *trans*,*cis*-IrCL(H)$_2$(CO)(PPh$_3$)$_2$ but much stronger than the Ir–CH$_3$ bond in *trans*,*cis*-Ir(Cl)(I)(CH$_3$)(CO)(PPh$_3$)$_2$ by 35 kcal mol^{-1} [25], where Bcat represents a catecholboryl group. The difference between M–CH$_3$ and M–B(OH)$_2$ bonds arises from the boryl p_π orbital. This orbital participates in the π-back donating interaction between M d_π and boryl p_π orbitals, as schematically shown in Scheme 2B. Actually, the electron population of the boryl p_π orbital is larger in the Pt(II) complex than that of the free boryl radical (0.287e), as follows: 0.326e in *cis*-PdH[B(OH)$_2$](PH$_3$)$_2$ and 0.366e in *cis*-PtH[B(OH)$_2$](PH$_3$)$_2$. This is clear evidence of π-back donation. The other factor is the orbital overlap. As shown in Table 6, the B(OH)$_2$ sp^2 orbital provides much larger overlap integrals than does the CH$_3$ sp^3 orbital. This is probably because the Pt–B bond distance is shorter than the Pt–C distance, as shown in Fig. 2. Why is the Pt–B distance shorter than the Pt–C distance? Again, the π-back donating interaction would be a main reason for the short Pt–B distance. Thus, the π-back donating interaction contributes to the M–B(OH)$_2$ bond not only in a direct way but also in an indirect way in which the π-back donating interaction shortens the M–B distance to increase orbital overlaps.

In *cis*-Pt[B(OH)$_2$](XH$_3$)(PH$_3$)$_2$, the Pt–PH$_3$ bond at a position *trans* to B(OH)$_2$ is much longer than that at a position *trans* to XH$_3$, as shown in Fig. 2. From this structure, it is reasonably concluded that the boryl ligand exhibits a stronger *trans* influence than the XH$_3$ ligand. The strong *trans* influence should also be noted as a characteristic feature of the boryl group.

5. Participation of the boryl p_π orbital in σ-bond activation

In our previous theoretical work on C–H σ-bond activation of dicyanomethane by Pd(0) complexes [15b], we showed that the empty π* orbital of the CN group stabilized the transition state through CT interaction with the occupied d orbital of Pd. The empty p_π orbital of the boryl group is expected to play the same role as the CN π* orbital. It is of considerable interest to investigate whether or not the empty p_π orbital of the boryl group participates in stabilization of the transition state of σ-bond activation.

We theoretically investigated σ-bond activation of methylborane CH$_3$–B(OH)$_2$ by Pt(PH$_3$)$_2$ [17]. The transition state structure is nearly planar, as shown in Fig. 3A, in which the dihedral angle between the B–C bond and the P–Pt–P plane is 20°. This structure is completely different from that of C–C σ-bond activation in which the C–C bond is almost perpendicular to the P–Pt–P plane (see Fig. 3D). The planar structure agrees with the expectation from the orbital interaction diagram shown in Scheme 3; the σ* orbital tends to take a position that provides a good overlap with the HOMO of Pt(PH$_3$)$_2$, because the charge-transfer from the metal d_π orbital to the σ* orbital must occur in this kind of σ-bond activation reaction to break the σ-bond. In the planar transition state, the σ* orbital can overlap well with the Pt d_{xz} orbital which is the HOMO of Pt(PH$_3$)$_2$ (Scheme 3). This means that the planar transition state structure is more favorable than the non-planar one. Also, the other reason is that the transition state is rather late; our previous study of C–Si σ-bond activation showed that the transition state was completely non-planar and the geometry change to the planar structure occurred at a late stage of the reaction [15a]. For these two reasons, the transition state structure of the B–C σ-bond activation is planar. This planar transition state, however, changes to the non-planar structure upon replacing PH$_3$ with a more bulky phosphine such as PH$_2$Et (see Fig. 3A). This is because the non-planar transition state structure is more favorable than the planar structure due to smaller steric repulsion. These results clearly suggest

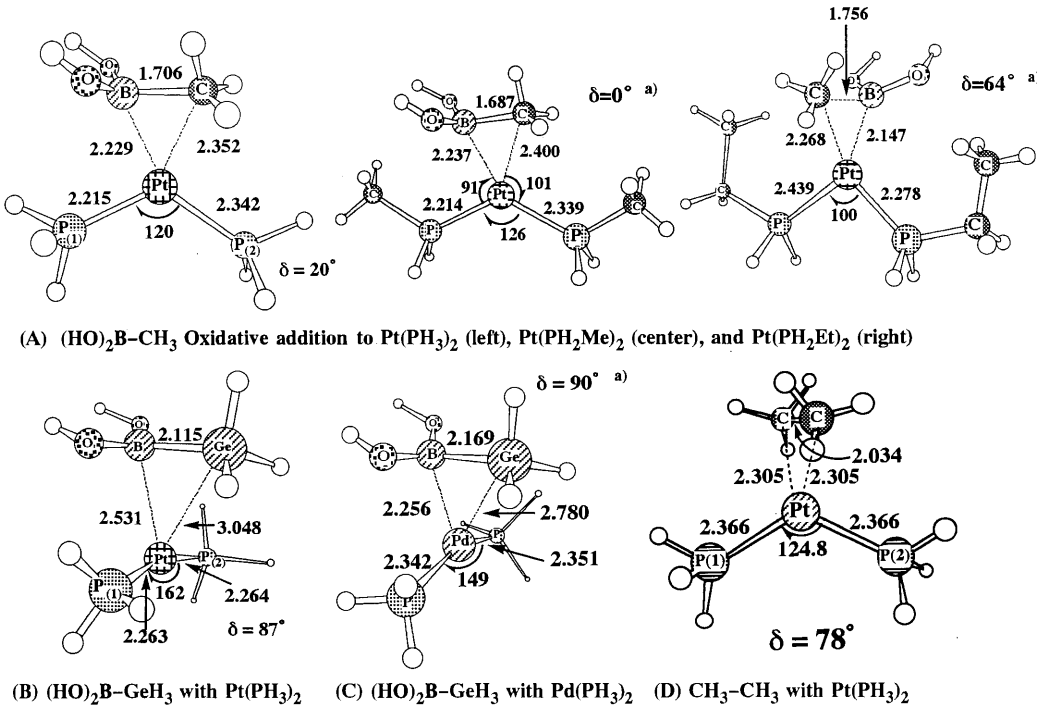

Fig. 3. Transition state structures of σ-bond activations of $(HO)_2B–CH_3$, $(HO)_2B–GeH_3$, and $CH_3–CH_3$ by $Pt(PH_3)_2$. Bond lengths in Å and bond angles in degrees. The δ value represents the dihedral angle between the σ-bond and the P–Pt–P plane.

that the transition state structure is sensitive to steric and electronic factors. Here, we stop and return to our main discussion, since this issue is not directly related to the chemistry of inter-element linkage.

In the σ-bond activation of $(HO)_2B–GeH_3$, the transition state is completely non-planar, as shown in Fig. 3B,C. One reason is that the steric repulsion becomes large because the GeH_3 group is larger than the CH_3 group, and the other reason is that the transition state is more reactant-like in B–Ge σ-bond activation than in B–C σ-bond activation.

Activation barriers (E_a) and reaction energies (ΔE) of these σ-bond activation reactions are summarized in Table 7. The B–Si, B–Ge, and B–Sn σ-bond activations by platinum(0) and palladium(0) complexes occur with either no barrier or nearly no barrier. On the other hand, B–C σ-bond activation by the platinum(0) complex requires a considerably large activation barrier. Moreover, this σ-bond activation by the palladium(0) complex cannot occur, and the reverse reaction, the B–C reductive elimination of $Pd(CH_3)[B(OH)_2](PH_3)_2$, occurs with no barrier. These results are interpreted in terms of the Pt–CH_3 and Pd–CH_3 bond strengths. Since the Pt–CH_3 bond is much weaker than the Pt–SiH_3, Pt–GeH_3, and Pt–SnH_3 bonds, B–C σ-bond activation by the platinum(0) complex occurs much less easily than the B–Si, B–Ge, and B–Sn σ-bond activations. The B–C σ-bond activation by the palladium(0) complex is much more difficult, because the Pd–CH_3 bond is much weaker than the Pt–CH_3 bond (vide supra).

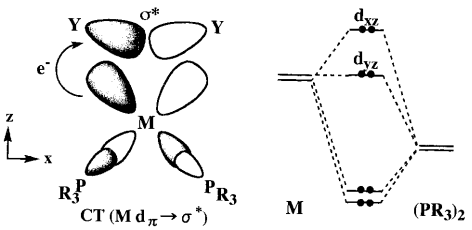

Scheme 3.

Table 7
Activation energy (E_a) and reaction energy (ΔE) of the B–X σ-bond activation by $M(PH_3)_2$ (M = Pd or Pt) (MP4(SDQ) in kcal mol^{-1}) [a]

	$(HO)_2B–XH_3$				$CH_3–CH_3$
	CH_3	SiH_3	GeH_3	SnH_3	
$Pd(PH_3)_2$					
E_a		1.2	1.1	no	
ΔE	(26) [b]	−13.7	−14.1	−22.4	
$Pt(PH_3)_2$					
E_a	21.5	no	2.2	no	57.4
ΔE	3.0	−33.0	−33.9	−39.4	7.6

[a] CCSD(T) in kcal mol^{-1}. The MP4(SDQ) method yields almost the same value as the CCSD(T) method.

[b] Optimization was carried out with the P–Pd–P angle assumed to be the same as that in the Pt analogue.

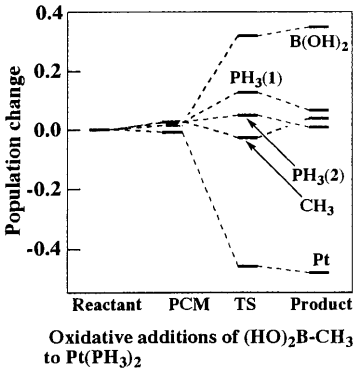

Fig. 4. The population changes in the σ-bond activation of $(HO)_2B–CH_3$ by $Pt(PH_3)_2$. A positive value represents an increase in the natural bond orbital population [21], and vice versa.

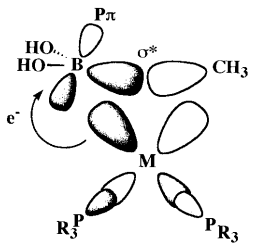

Scheme 4.

It should be noted here that the B–C σ-bond activation occurs with a smaller activation energy than the C–C σ-bond activation (see Table 7). Population changes in the reaction are shown in Fig. 4 [17]. Interestingly, the electron population of the boryl group increases significantly in the precursor complex and the transition state. This suggests that the boryl group participates in the CT interaction with the occupied d orbital of Pt. In the transition state, the boryl σ* orbital overlaps with the Pt d orbital, and at the same time, the boryl p_π orbital can overlap with the same Pt d orbital to enhance the π-back donating interaction, as shown in Scheme 4. Because of this additional interaction, the CT interaction becomes stronger and the transition state is more stabilized than that of C–C σ-bond activation. Thus, B–C σ-bond activation occurs much more easily than C–C σ-bond activation.

6. Hypervalency of Si, Ge, and Sn in the reaction

Though hypervalency of these elements has often been observed in stable molecules, its observation in reaction has been rather limited. It is worthwhile to clarify the participation of hypervalency in the reaction. To investigate the contribution of hypervalency in the reaction, we theoretically investigated the reductive elimination of $Pd(XH_3)(\eta^3\text{-}C_3H_5)(PH_3)$, where $XH_3 = CH_3$, SiH_3, GeH_3, and SnH_3 [16].

$$Pd(XH_3)(\eta^3\text{-}C_3H_5)(PH_3) \rightarrow Pd(PH_3)(CH_2{=}CH{-}CH_2{-}XH_3) \quad (9)$$

Typical geometry changes of these reactions are shown in Fig. 5, in which geometry changes of $C_3H_5–GeH_3$ and $C_3H_5–SnH_3$ reductive eliminations are omitted because they are similar to the geometry changes of $C_3H_5–SiH_3$ reductive elimination. Interesting features are observed in the transition state; in the reductive elimination of $C_3H_5–CH_3$, the $Pd–CH_3$ bond considerably lengthens, while the $C_3H_5–CH_3$ distance is still much longer than the usual C–C bond. On the other hand, the $Pd–SiH_3$, $Pd–GeH_3$, and $Pd–SnH_3$ distances lengthen only slightly in the transition states, while the $C_3H_5–SiH_3$, $C_3H_5–GeH_3$, and $C_3H_5–SnH_3$ distances are similar to those of the products: In other words, the SiH_3, GeH_3, and SnH_3 groups can form a new bond with allyl carbon atom, keeping the bonding interaction with Pd. This feature is considered to arise from hypervalency of Si, Ge, and Sn elements. Actually, we can understand from the geometry changes of Fig. 5 that the Si, Ge, and Sn elements take a five-coordinate structure in the transition state, as shown in Scheme 5.

In spite of the large exothermicity, the $C_3H_5–CH_3$ reductive elimination requires a very large E_a value (Table 8). This is consistent with the transition state structure in which the allyl–methyl distance is still long and the Pd–methyl bond is much lengthened. However, the other reductive eliminations take place with a moderate E_a value, which is consistent with their transition state structures where the allyl–XH_3 distance is similar to that of the product and the $Pd–XH_3$ bond is moderately lengthened. These reactions are much less exothermic for X = Si and Ge than the $CH_3–C_3H_5$ reductive elimination and slightly endothermic for X = Sn. The above results suggest that the bond energy is not responsible for the large E_a value of $C_3H_5–CH_3$ reductive elimination. We examined the distortion energies which arise from the geometry changes of the allyl moiety, $Pd–XH_3$ bond lengthening, and the direction change of XH_3, as shown in Fig. 6, where the distortion energy is defined as an energy difference between the equilibrium structure and the distorted geometry in the transition state. The distortion energy $E_{dist}(1)$ of the allyl moiety is not very different among CH_3, SiH_3, GeH_3, and SnH_3. The distortion energy $E_{dist}(2)$ caused by $Pd–CH_3$ bond lengthening is moderately larger than those of the others. On the other hand, the distortion energy $E_{dist}(3)$ caused by the direction change of CH_3 is much larger than those of the others. These results clearly indicate that the large E_a value of $C_3H_5–CH_3$ reductive elimination arises from the large distortion energy by the direction change of CH_3. If the X atom could form an extra bonding interaction in any direction, direction change of XH_3 would easily occur without considerable energy destabilization. In other words, when the X

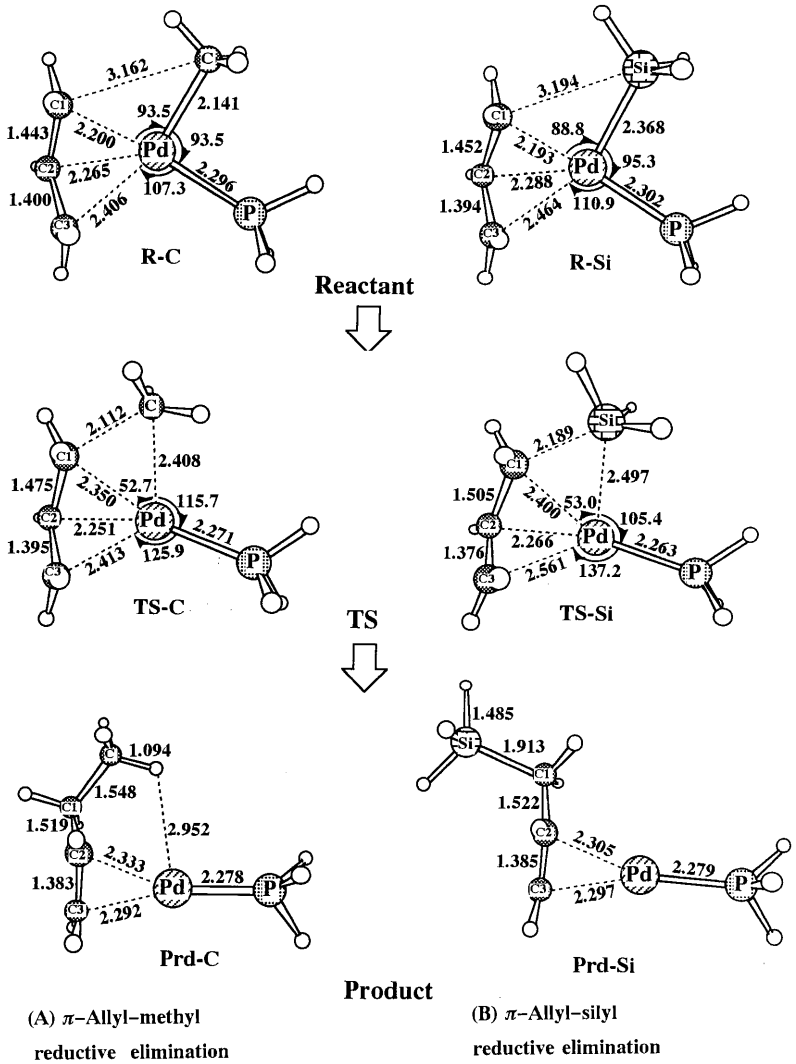

Fig. 5. Geometry changes of the allyl–methyl and allyl–silyl reductive eliminations from Pd(η^3-C_3H_5)(XH_3)(PH_3) (X = C or Si). Bond lengths in Å and bond angles in degrees [16].

element has hypervalency, the XH_3 group would change easily its direction and would form a new bonding interaction with an allyl carbon atom, keeping the Pd–XH_3 bond. Thus, the following conclusions are reasonable: (i) the small $E_{dist}(3)$ values of Si, Ge, and Sn systems arise from the hypervalency of Si, Ge, and Sn elements, (ii) allyl–silyl, allyl–germyl, and allyl–stannyl reductive eliminations occur easily because of the hypervalency of Si, Ge, and Sn elements, and (iii) the allyl–methyl reductive elimination requires a large activation energy because of the absence of hypervalency.

Our previous calculations clearly showed that the allyl–hydrogen reductive elimination of Pd(H)(η^3-C_3H_5)(PH_3) easily occurred with a very small activation barrier [26]. Though the H atom does not have hyper-

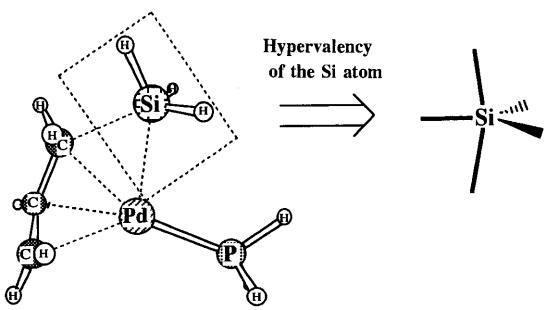

Scheme 5.

Table 8
An activation energy (E_a) and a reaction energy (ΔE) of the allyl–XH_3 reductive elimination of Pd(XH_3)(η^3-C_3H_5)(PH_3) (X = C, Si, Ge, or Sn) [a]

	C	Si	Ge	Sn
E_a	23.3	11.6	12.6	10.9
ΔE	−30.1	−8.2	−3.7	3.8

[a] CCSD(T) in kcal mol^{-1}.

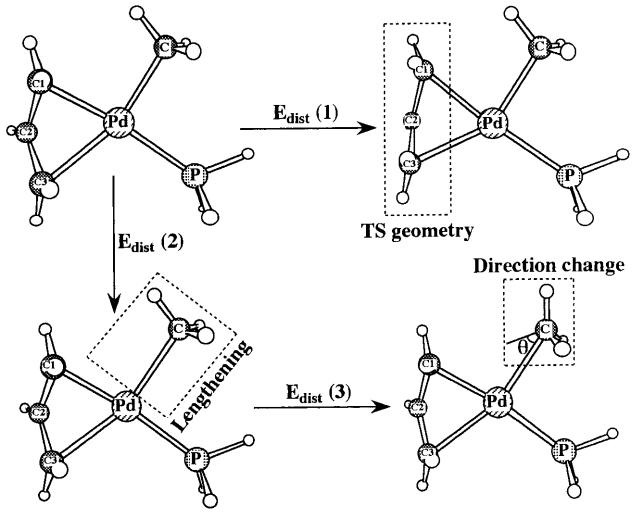

	$E_{dist}(1)$	$E_{dist}(2)$	$E_{dist}(3)$
CH_3	2.6	7.3	22.0
SiH_3	6.4	1.2	13.8
GeH_3	6.0	2.0	11.7
SnH_3	6.0	2.9	11.1

(MP4(SDQ); kcal/mol)

Fig. 6. Distortion energies (energy difference between the equilibrium structure and the distorted structure taken in the transition state (CCSD(T) method, kcal mol^{-1})) induced by the geometry changes of η^3-allyl moiety $E_{dist}(1)$, the Pd–XH_3 bond lengthening $E_{dist}(2)$, and the direction change of the XH_3 group $E_{dist}(3)$.

valency, the H atom can form a two-electron three-center interaction. In other words, the H atom can start to form a new bonding interaction with an allyl carbon atom, keeping the Pd–H bond. Thus, not only the hypervalency but also the two-electron three-center interaction plays an important role to facilitate the σ-bond activation reaction and its reverse reaction.

7. Conclusions

In this short account, we presented the characteristic features of the boryl group in bonding interactions and reaction processes. In both, the empty p_π orbital of the boryl group plays an important role; for instance, it participates in the hyperconjugation with the methyl C–H bond, which leads to the stronger boryl–methyl bond than the methyl–methyl bond. Also, the empty p_π orbital participates in the intramolecular CT interaction with silyl, germyl, and stannyl bonds. In the σ-bond activation reaction of methylborane, silylborane, germylborane, and stannylborane, the boryl p_π orbital can form a CT interaction with the metal d orbital, to stabilize the transition state. As a result, the activation reaction of these σ-bonds easily occurs.

The Si, Ge, and Sn elements exhibit interesting features in the bonding nature and the transition state of σ-bond activation reaction. The M–SiH_3, M–GeH_3, and M–SnH_3 bonds (M = Pd or Pt) are much stronger than the M–CH_3 bond. This result is reasonably interpreted in terms of the less expansion of the sp^3 orbital of CH_3 and the higher energy level of the CH_3 sp^3 electron when CH_3 is significantly negatively charged. The M–XH_3 bond becomes weaker in the order M–SiH_3 > M–GeH_3 > M–SnH_3. This is because the XH_3 sp^3 orbital becomes higher in energy in the order SiH_3 < GeH_3 < SnH_3 and the overlap integrals between XH_3 sp^3 and M valence orbitals decrease slightly in the order SiH_3 > GeH_3 > SnH_3. In the reductive elimination of Pd(XH_3)(η^3-C_3H_5)(PH_3) (and the reverse reaction, i.e. σ-bond activation reaction), the silyl, germyl, and stannyl groups can form an allyl–XH_3 bond without Pd–XH_3 bond breaking because of the hypervalency of Si, Ge, and Sn elements. As a result, the σ-bond involving these elements easily undergoes the σ-bond activation and its reverse reductive elimination. However, the reductive elimination of Pd(CH_3)(η^3-C_3H_5)(PH_3) requires a very large E_a value, in spite of the large exothermicity, because of the absence of hypervalency of the C atom.

Acknowledgements

This work was financially supported in part by a Grant-in-Aid on Scientific Research on Priority Areas Inter-element Chemistry and Molecular Physical Chemistry.

References

[1] (a) I. Ojima, in: S. Patai, Z. Rappoport (Eds.), The Chemistry of Organic Silicon Compounds, Part II, Wiley, Chichester, 1989, Chapter 25. (b) T.D. Tilley, in: S. Patai, Z. Rappoport (Eds.), The Chemistry of Organic Silicon Compounds, Part II, Wiley, Chichester, 1989, Chapter 24.
[2] K. Burgess, M.J. Ohlmeyer, Chem. Rev. 91 (1991) 1179.
[3] H.K. Shama, K.H. Pannell, Chem. Rev. 95 (1995) 1351.
[4] (a) T. Ishiyama, N. Matsuda, N. Miyaura, A. Suzuki, J. Am. Chem. Soc. 115 (1993) 11018. (b) T. Ishiyama, N. Matsuda, N. Murata, F. Ozawa, A. Suzuki, N. Miyaura, Organometallics 15 (1996) 713.
[5] (a) H. Okinoshima, K. Yamamoto, M. Kumada, J. Am. Chem. Soc. 94 (1972) 9263. (b) K. Tamao, T. Hayashi, M. Kumada, J. Organomet. Chem. 114 (1976) C19.
[6] K.A. Horn, Chem. Rev. 95 (1995) 1317.
[7] Y. Ito, M. Suginome, M. Murakami, J. Org. Chem. 56 (1991) 1948.
[8] (a) H. Yamashita, M. Catellani, M. Tanaka, Chem. Lett. (1991) 241. (b) T. Hayashi, H. Yamashita, T. Sakakura, Y. Uchimaru, M. Tanaka, Chem. Lett. (1991) 245.
[9] (a) M. Suginome, H. Nakamura, Y. Ito, J. Chem. Soc. Chem. Commun. (1996) 2777. (b) M. Suginome, H. Nakamura, T.

Matsuda, Y. Ito, J. Am. Chem. Soc. 120 (1998) 1229. (c) M. Suginome, H. Nakamura, Y. Ito, Angew. Chem. Int. Ed. Engl. 36 (1997) 2516.
[10] S. Onozawa, Y. Hatanaka, N. Choi, M. Tanaka, Organometallics 16 (1997) 5389.
[11] (a) S. Obara, K. Kitaura, K. Morokuma, J. Am. Chem. Soc. 106 (1984) 7482. (b) N. Koga, K. Morokuma, J. Phys. Chem. 94 (1990) 5454. (c) N. Koga, K. Morokuma, J. Am. Chem. Soc. 115 (1993) 6883. (d) T. Matsubara, N. Koga, D.G. Musaev, K. Morokuma, J. Am. Chem. Soc. 120 (1998) 12692.
[12] J.J. Low, W.A. Goddard, J. Am. Chem. Soc. 108 (1986) 6115. J.J. Low, W.A. Goddard, Organometallics 5 (1986) 609.
[13] (a) P.E.M. Siegbahn, J. Am. Chem. Soc. 118 (1996) 1487. (b) P.E.M. Siegbahn, R.H. Crabtree, J. Am. Chem. Soc. 118 (1996) 4442. (c) M.R.A. Blomberg, P.E.M. Siegbahn, M. Svensson, J. Am. Chem. Soc. 114 (1992) 6095. (d) P.E.M. Siegbahn, M.R.A. Blomberg, Organometallics 13 (1994) 354 and refs. therein.
[14] (a) S. Niu, M.B. Hall, J. Am. Chem. Soc. 120 (1998) 6169. (b) R.J. Catano, M.B. Hall, Organometallics 15 (1996) 1889.
[15] (a) S. Sakaki, N. Mizoe, Y. Musashi, B. Biswas, M. Sugimoto, J. Phys. Chem. A 102 (1998) 8027. (b) S. Sakaki, B. Biswas, M. Sugimoto, Organometallics 17 (1998) 1278.
[16] B. Biswas, M. Sugimoto, S. Sakaki, Organometallics 18 (1999) 4015.
[17] S. Sakaki, S. Kai, M. Sugimoto, Organometallics 18 (1999) 4825.
[18] (a) S. Sakaki, N. Mizoe, M. Sugimoto, Organometallics 17 (1998) 2510. (b) S. Sakaki, N. Nizoe, Y. Musashi, M. Sugimoto, J. Mol. Struc. (Theochem), 461–462 (1999) 533. (c) S. Sakaki, N. Mizoe, M. Sugimoto, Y. Musashi, Coord. Chem. Rev. 190–191 (1999) 933.
[19] (a) S. Sakaki, M. Ogawa, Y. Musashi, T. Arai, J. Am. Chem. Soc. 116 (1994) 7258. (b) M. Sugimoto, I. Yamasaki, N. Mizoe, M. Anzai, S. Sakaki, Theor. Chem. Acc. 102 (1999) 307.
[20] Q. Cui, D.G. Musaev, K. Morokuma, Organometallics 16 (1997) 1355.
[21] A.E. Reed, R.B. Winestock, F. Weinhold, J. Chem. Phys. 83 (1985) 735. A.E. Reed, L.A. Curtis, F. Weinhold, Chem. Rev. 88 (1988) 899.
[22] S. Sakaki, K. Masunaga, Y. Ijiri, M. Sugimoto, to be published.
[23] C.N. Iverson, M.R. Smith, III, J. Am. Chem. Soc. 117 (1995) 4403.
[24] S. Sakaki, T. Kikuno, Inorg. Chem. 36 (1997) 226.
[25] P.R. Rablen, J.F. Hartwig, J. Am. Chem. Soc. 116 (1994) 4121.
[26] S. Sakaki, H. Satoh, H. Shono, Y. Ujino, Organometallics 15 (1996) 1713.
[27] L.A. Curtis, K. Raghavachari, J.A. Pople, J. Chem. Phys. 98 (1993) 1293.
[28] L.A. Curtiss, K. Raghavachari, P.C. Redfern, V. Rassolov, J.A. Pople, J. Chem. Phys. 109 (1998) 7764.